PHYSICS

Novel excitations near quantum criticality in geometrically frustrated antiferromagnet $CsFeCl_3$

Shohei Hayashida[1]*, Masashige Matsumoto[2], Masato Hagihala[1†], Nobuyuki Kurita[3], Hidekazu Tanaka[3], Shinichi Itoh[4], Tao Hong[5], Minoru Soda[1‡], Yoshiya Uwatoko[1], Takatsugu Masuda[1§]

The investigation of materials that exhibit quantum phase transition provides valuable insights into fundamental problems in physics. We present neutron scattering under pressure in a triangular-lattice antiferromagnet that has a quantum disorder in the low-pressure phase and a noncollinear structure in the high-pressure phase. The neutron spectrum continuously evolves through critical pressure; a single mode in the disordered state becomes soft with the pressure and it splits into gapless and gapped modes in the ordered phase. Extended spin-wave theory reveals that the longitudinal and transverse fluctuations of spins are hybridized in the modes because of noncollinearity, and previously unidentified magnetic excitations are formed. We report a new hybridization of the phase and amplitude fluctuations of the order parameter near a quantum critical point in a spontaneously symmetry-broken state.

INTRODUCTION

For understanding condensed matter, investigation of collective excitation in the low energy range is indispensable. According to quantum field theory, excitation in a system with spontaneously symmetry breaking is characterized by phase and amplitude fluctuations of order parameters. The former is known as the Nambu-Goldstone (NG) mode, and the latter is called as the amplitude mode. Although these modes are usually separated, they are hybridized under some conditions, and interesting phenomena are induced; for example, in a crystal lattice system, acoustic phonon (NG mode) and optical phonon (amplitude mode) are hybridized through anharmonic terms in a thermoelectric material PbTe, which renormalizes the phonon spectrum and leads to low thermal conductivity and high figure of merit in thermoelectric property (*1*). Such a hybridization effect could exist in other types of elementary excitations; however, no research has been reported to our knowledge. One of the reasons is that the amplitude mode itself is not trivial in other systems: superconductors (*2*), charge density wave (*3*), ultracold atoms (*4*), and insulating antiferromagnets. The existence of the amplitude mode in the antiferromagnets requires strong fluctuation of the magnetic moment and the system location near a quantum critical point (QCP). So far, it has been found in a number of spin systems free from geometrical frustration such as quasi–one-dimensional chains (*5*, *6*), dimer (*7*–*9*), square lattice (*10*), and two-leg ladder antiferromagnet (*11*). In magnets, in the presence of geometrical frustration that could induce the hybridization of modes, magnon excitations from ordered states have been less focused these days (*12*), although fractional excitations in the spin liquid were intensively studied (*13*–*15*). In particular, the collective excitations from a noncollinear spin structure in a geometrical frustrated lattice near QCP have not been studied, and its investigation is of primary importance to find a novel state and to advance the physics of the frustration and quantum criticality.

Spin $S = 1$ easy-plane antiferromagnet is one of the prototypical quantum spin systems that allows exploring the nature of the quantum phase transition (QPT) (*16*, *17*). The Hamiltonian is expressed by $\mathcal{H} = \sum_i D(S_i^z)^2 + \sum_{i,j} J_{ij} \boldsymbol{S}_i \cdot \boldsymbol{S}_j$, where $\boldsymbol{S}_i$ is the spin operator at the i site. The first term D is positive and gives an easy-plane single-ion anisotropy. The second term is a Heisenberg interaction with $J_{ij} > 0$ for an antiferromagnetic coupling. The positive D splits the triplet $S = 1$ states into the singlet ground state $S^z = 0$, and the doublet excited states $S^z = \pm 1$,

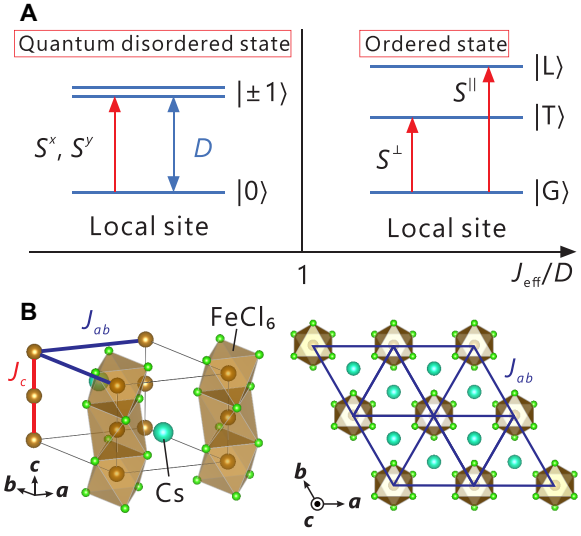

Fig. 1. Spin $S = 1$ easy-plane antiferromagnet. (**A**) Schematic diagram of the $S = 1$ easy-plane antiferromagnet. In the ordered state, the doublet excited states $|\pm 1\rangle$ splits into $|\mathrm{L}\rangle$ and $|\mathrm{T}\rangle$. Here, the former and latter have longitudinal and transverse fluctuations, respectively. (**B**) Crystal structure of $CsFeCl_3$ with the space group $P6_3/mmc$ (*30*). Magnetic Fe^{2+} ions having pseudospin $S = 1$ form one-dimensional chains along the crystallographic c axis, and the chains form the triangular lattice in the ab plane. Red and blue lines indicate the intrachain interaction J_c and interchain/intratriangle interaction J_{ab}, respectively.

[1]Institute for Solid State Physics, The University of Tokyo, Chiba 277-8581, Japan. [2]Department of Physics, Shizuoka University, Shizuoka 422-8529, Japan. [3]Department of Physics, Tokyo Institute of Technology, Meguro-ku, Tokyo 152-8551, Japan. [4]Neutron Science Division, Institute of Materials Structure Science, High Energy Accelerator Research Organization, Tsukuba, Ibraki 305-0801, Japan. [5]Neutron Scattering Division, Oak Ridge National Laboratory, Oak Ridge, TN 37831, USA.
*Present address: Laboratory for Solid State Physics, ETH Zürich, Switzerland.
†Present address: Institute of Materials Structure Science, High Energy Accelerator Research Organization, Tsukuba, Japan.
‡Present address: RIKEN Center for Emergent Matter Science, Wako, Japan.
§Corresponding author. Email: masuda@issp.u-tokyo.ac.jp

and it favors a quantum disordered (QD) state as shown on the left in Fig. 1A. By contrast, the spin interaction J_{ij} allows the system to cause a magnetic long-range order (LRO).

In the LRO phase, the energy eigenstates change as shown on the right in Fig. 1A. Here, $|G\rangle$ is the ground state, while $|T\rangle$ and $|L\rangle$ are excited states. They are given by $|G\rangle = u|0\rangle + v/\sqrt{2}(|1\rangle + |-1\rangle)$, $|T\rangle = 1/\sqrt{2}(-|1\rangle + |-1\rangle)$, and $|L\rangle = -v|0\rangle + u/\sqrt{2}(|1\rangle + |-1\rangle)$ with $u^2 + v^2 = 1$; u and v are determined by D and J_{ij}. In the ordered phase, $v \neq 0$ and a finite magnetic moment appears in the *ab* plane (*16*, *17*). We separate the spin operator into longitudinal ($S^{\parallel}$) and transverse ($S^{\perp}$) components relative to the local ordered moment. A remarkable feature is that the second excited state $|L\rangle$ can be excited only by the longitudinal component $S^{\parallel}$, while the first one $|T\rangle$ can be excited by the transverse component $S^{\perp}$.

Thus, the excited states at a local site are separated into two states having longitudinal and transverse fluctuations. The studies in the square lattice predicted an enhanced amplitude/longitudinal mode as a one-magnon excitation in addition to the NG/transverse mode in the LRO phase near the QCP (*10*, *16*). In the collinear magnetic structure, in general, the transverse and longitudinal fluctuations are not hybridized, and they are separated (*5*–*11*). In the geometrically frustrated spin system, on the other hand, these fluctuations could be hybridized because of the noncollinearity of the magnetic structure. This point was theoretically investigated in the continuum-like spectra in the $S = 1/2$ and $S = 3/2$ systems, where the longitudinal fluctuation stems from two-magnon process (*18*). Since $S = 1$ easy-plane antiferromagnet has the longitudinal fluctuation in one-magnon process, in contrast, the two fluctuations hybridize in one-magnon level, and a novel excited state may appear as a well-defined eigen mode. Details of such a study, however, have not been reported either in experiment or theory.

$CsFeCl_3$ is a model material for the $S = 1$ easy-plane triangular antiferromagnet as shown in Fig. 1B. The inelastic neutron scattering (INS) study at ambient pressure revealed that the ferromagnetic chains along the *c* axis are antiferromagnetically coupled in the *ab* plane (*19*). The ground state is the QD state because of large single-ion anisotropy. The magnetic susceptibility measurement under pressures exhibited a

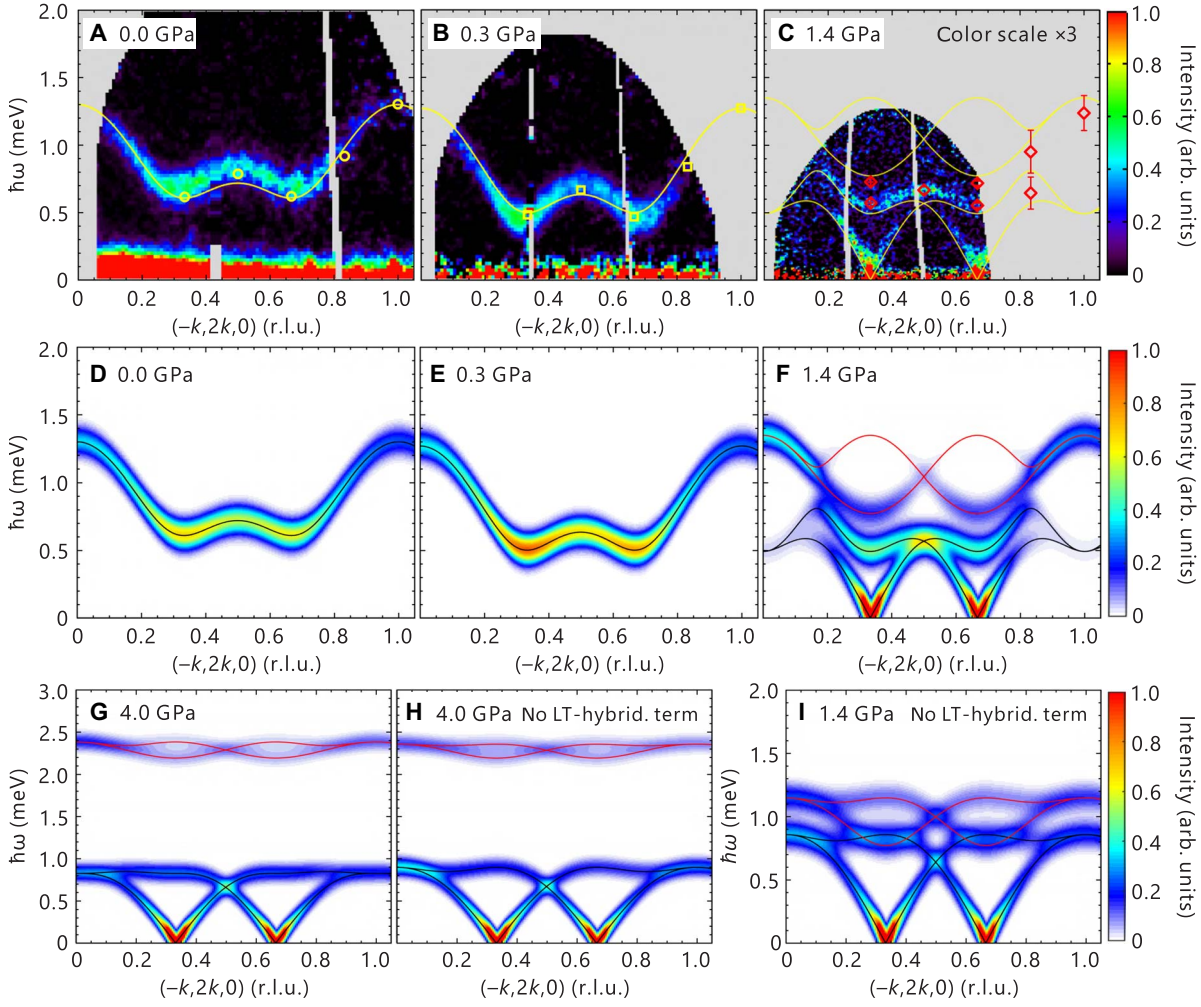

Fig. 2. Inelastic neutron scattering spectra. The spectra obtained at a chopper spectrometer under (**A**) 0.0 GPa at 6 K, (**B**) 0.3 GPa at 2.7 K, and (**C**) 1.4 GPa at 0.9 K sliced by the energy transfer – wave vector ($\hbar\omega - \boldsymbol{q}$) plane for $\boldsymbol{q} = (-k, 2k, 0)$. The yellow circles, squares, and red diamonds are the peak positions of the excitations obtained from the constant-$\boldsymbol{q}$ scans using a triple-axis spectrometer. The solid yellow curves are the dispersions calculated by ESW. Calculated neutron cross section by the ESW under (**D**) 0.0 GPa, (**E**) 0.3 GPa, (**F**) 1.4 GPa, and (**G**) 4.0 GPa at 0 K. Calculated neutron cross section in the absence of the cross term in Eq. 2 under (**H**) 4.0 GPa and (**I**) 1.4 GPa at 0 K. The black and red solid curves in (F) to (I) are gapless and gapped modes, respectively. More detailed pressure dependence of the calculated spectra is shown in fig. S3.

pressure-induced magnetic order above a critical pressure of about 0.9 GPa (*20*). Because of the strong easy-plane anisotropy, the ordered moment aligns in the *ab* plane; the neutron diffraction evidenced the noncollinear 120° structure in the LRO phase (*21*). $CsFeCl_3$ is, thus, a promising host for the pressure-induced QPT in the geometrically frustrated lattice.

RESULTS

INS spectra of $CsFeCl_3$ under hydrostatic pressures

The INS spectrum measured at 0.0 GPa by using a chopper spectrometer in Fig. 2A exhibits a single dispersive excitation with the energy gap of 0.6 meV at the wave vectors $\boldsymbol{q} = (-k, 2k, 0)$ for $k = 1/3$ and 2/3, which is consistent with a previous report (*19*). The energy gap at 0.3 GPa in Fig. 2B becomes softened when approaching the ordered state (*21*). A qualitatively different spectrum is observed in the ordered state at 1.4 GPa in Fig. 2C. A well-defined gapless excitation emerges at $k = 1/3$ and 2/3, and another dispersive excitation with the minimum energy transfer (ħω) of about 0.55 meV is observed in the higher energy range.

Detailed structure of INS spectra

The INS spectra at 1.4 GPa were collected by using a triple-axis spectrometer to cover wide ħω to $\boldsymbol{q}$ range as shown in Fig. 3A. The spectral lineshapes at $k = 1/3$ and 2/3 are fitted by double Lorentzians convoluted by experimental resolution functions. The excitation becomes broad at $k = 5/6$, where four peaks are expected as shown in Fig. 2C. Because it is difficult to resolve it into four peaks, we used the convoluted double Loretzians. The extracted peak energies are overplotted in Fig. 2C with red diamonds.

Although the linewidth is large, the extracted dispersion relation and the momentum dependence of the intensity are consistent with the theoretical result, as shown in fig. S5. The details of convolution calculation are described in section S4.

The pressure evolution of the energy gap at $\boldsymbol{q} = (-1/3, 2/3, 0)$ is shown in Fig. 3B. The excitations at 0.0, 0.3, and 0.6 GPa show that the gap is suppressed with an increase in pressure. At 0.8, 0.9, and 1.1 GPa, the gap position cannot be identified, and the broad excitations are observed below 1.0 meV. This implies that the system is near the QCP at these pressures. At 1.4 GPa, the excitation appears at 0.55 meV, which corresponds to the high energy mode in Fig. 2C. The intensity of the excitation at 1.4 GPa in Fig. 3B is weak compared with those in the QD phase. This is because most of the magnetic intensity is concentrated at the magnetic Bragg peak owing to the LRO. The energies of the gap at 0.0, 0.3, and 0.6 GPa and the transition temperatures obtained both in the present and previous (*21*) studies are plotted in Fig. 3C.

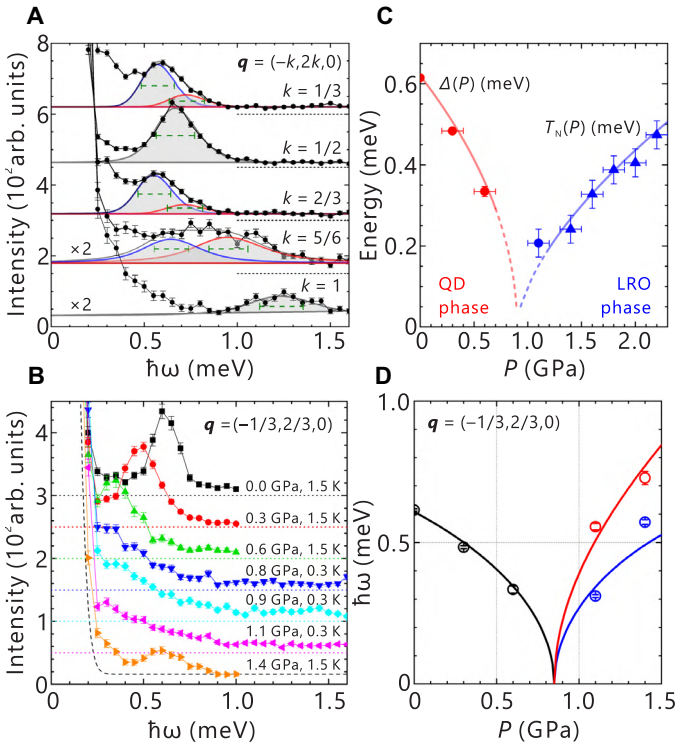

Fig. 3. Detailed structure of INS spectra. (**A**) Constant-$\boldsymbol{q}$ scans at (−*k*, 2*k*, 0) under 1.4 GPa measured at a triple-axis spectrometer. Blue and red curves are the fitting results by Lorentzians convoluted by the instrumental resolution function. Green dashed bars indicate the experimental resolution. (**B**) Pressure evolutions of the constant-$\boldsymbol{q}$ scans at (−1/3, 2/3, 0) obtained at a triple-axis spectrometer. The black dashed curve is a Gaussian function of the incoherent scattering at 1.4 GPa with the full width at half maximum of 0.17 meV. (**C**) Phase diagram of the pressure-induced QPT in $CsFeCl_3$, which is obtained from energy gaps Δ and transition temperatures T_N (*21*). Red and blue curves are guides for eyes. (**D**) Pressure dependence of the excitation energies at (−1/3, 2/3, 0) calculated by the ESW. Above 0.9 GPa, the blue and red curves are the excitations of gapless and gapped modes, respectively; the circles are peak energies evaluated from the constant-$\boldsymbol{q}$ scans.

DISCUSSION

To discuss the obtained spectra, the one-magnon cross section was calculated on the basis of the extended spin-wave (ESW) theory (*22*). It is equivalent to the harmonic bond-operator theory (*23*–*26*), and it is convenient to apply complex spin systems such as noncollinear ordered states (*17*). For $CsFeCl_3$, we study the following Hamiltonian

$$\mathcal{H} = \sum_i D(S_i^z)^2 + J_c \sum_{\langle i,j\rangle}^{\text{chain}} \boldsymbol{S}_i \cdot \boldsymbol{S}_j + J_{ab} \sum_{\langle i,j\rangle}^{\text{plane}} \boldsymbol{S}_i \cdot \boldsymbol{S}_j \quad (1)$$

where the sum is taken over the exchange interactions J_c and J_{ab} as shown in Fig. 1B. The relation between the crystallographic axes and the global *xyz* coordinate of the spin system is shown in Fig. 4A. Here, we focus on the last term and rewrite it as $\mathcal{H}_{ab} = \sum_{\langle i,j\rangle}^{\text{plane}} \mathcal{H}_{ij}^{ab}$ with $\mathcal{H}_{ij}^{ab} = J_{ab} \boldsymbol{S}_i \cdot \boldsymbol{S}_j$. Introducing creation and annihilation Bose operators for the local longitudinal ($|L\rangle$) and transverse ($|T\rangle$) excited states (*22*), we can see that $\mathcal{H}_{ij}^{ab}$ brings about the dynamics of the excited states as $\mathcal{H}_{ij}^{ab} = J_{ab} \sum_{mn=L,T} \langle m | \boldsymbol{S}_i | G\rangle \cdot \langle G | \boldsymbol{S}_j | n\rangle a_{im}^\dagger a_{jn}$. In the local ηζξ coordinates shown in Fig. 4B, $\mathcal{H}_{ij}^{ab}$ is expressed as

$$\mathcal{H}_{ij}^{ab} = J_{ab}[\cos\phi_{ij}(S_i^\eta S_j^\eta + S_i^\zeta S_j^\zeta) + S_i^\xi S_j^\xi + \sin\phi_{ij}(S_i^\eta S_j^\zeta - S_i^\zeta S_j^\eta)]. \quad (2)$$

Here, $\phi_{ij} = \phi_i - \phi_j$, and ϕ_i represents the angle of the magnetic moment at the *i* site. The first two (ηη + ζζ and ξξ) terms are diagonal for the $|L\rangle$ and $|T\rangle$ states, while the last off-diagonal (ηζ − ζη) term leads to hybridization between the $|L\rangle$ and $|T\rangle$ states (LT-hybridization). We will call it LT-hybridization term hereafter. For instance, the $|T\rangle$ state can move from the *j* site to the *i* site and change into the $|L\rangle$ state (see Fig. 4C). This process is described as $J_{ab}\sin\phi_{ij}\langle L | S_i^\eta | G\rangle\langle G | S_j^\zeta | T\rangle a_{iL}^\dagger a_{jT}$. In the same way, the pair creation

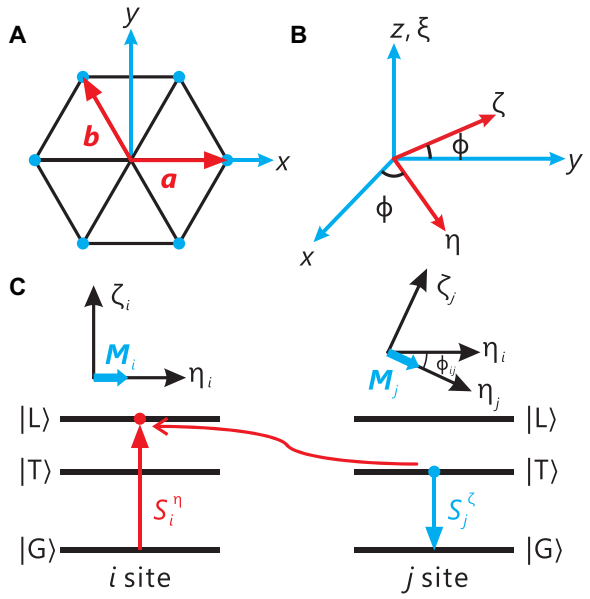

Fig. 4. Role of the LT-hybridization term. (**A**) Relation between the global *xyz* coordinate and the crystallographic axes. (**B**) Relationship between the global *xyz* coordinate and the local ηζξ coordinate. ϕ is the angle of the local magnetic moment measured from the *x* axis. η axis (ζ axis) is taken parallel (perpendicular) to the moment in the *ab* plane. (**C**) Schematic of transition from $|T\rangle$ state to $|L\rangle$ state via the intersite interaction. $\boldsymbol{M}_i$ represents the magnetic moment at the *i* site.

process is described as $J_{ab}\sin\phi_{ij}\langle L|S_i^\eta|G\rangle\langle T|S_j^\zeta|G\rangle a_{iL}^\dagger a_{jT}^\dagger$. The detailed description of the processes is summarized in fig. S2. We emphasize that one-magnon processes for the LT-hybridization can only exist in noncollinear states, i.e., $\sin\phi_{ij}\neq 0$ in Eq. 2.

Spin interactions and anisotropy are parametrized by comparing the experiment and calculation, and they are represented as a function of the pressure by the linear-interpolation as follows: J_c (meV) = $-0.5 - 0.14\times p$, J_{ab} (meV) = $0.0312 - 0.0015\times p$, and D (meV) = $2.345 + 0.365\times p$, where the p (GPa) is the value of pressure. The pressure dependencies of the excitation energies at $\boldsymbol{q}$ = (−1/3, 2/3, 0) are indicated by circles and solid curves in Fig. 3D. The data are reasonably reproduced by the calculation within the linear pressure dependence in J_c, J_{ab}, and D. The calculated dispersion relations obtained by using the extracted parameters are indicated by the solid yellow curves in Fig. 2 (A to C), and the calculation is consistent with the experiment both in the QD and LRO phases. Furthermore, the calculated INS spectra in Fig. 2 (D to F) also reproduce the observed ones.

To understand the effects of LT-hybridization, we demonstrate the INS spectra after dropping the LT-hybridization term in Eq. 2. The results are shown in Fig. 2 (H and I), where the gapless (gapped) modes are pure transverse (longitudinal) modes in this case. With an increase in pressure from 1.4 to 4.0 GPa, the longitudinal modes shift to the high-energy region and lose intensity, as in the collinear case of $TlCuCl_3$ (*8*). When LT-hybridization is taken into account, off-diagonal elements between the $|L\rangle$ and $|T\rangle$ states lead to level repulsion. Far from the QCP (p = 4.0 GPa), the INS spectrum is not affected by the hybridization [compare Fig. 2, G and H]. By contrast, the spectrum is strongly renormalized by the hybridization near the QCP (compare Fig. 2, F and I), and novel magnetic excitations are formed; both gapless and gapped modes are accompanied by strong longitudinal and transverse fluctuations. The shape of the INS spectrum resembles that in the QD phase (compare Fig. 2, E and F). Note that the spectrum continuously evolves through the QCP, and the property of the second-order phase transition is ensured by considering LT-hybridization. Thus, LT-hybridization plays an important role in magnon dynamics in noncollinear magnets near QCP. The INS measurements in $CsFeCl_3$ revealed this by the fine tuning of pressure through the QCP.

Since the newly found excitation exists in a noncollinear spin structure, the search of the excitation in different types of noncollinear structures such as cycloidal structure, all-in all-out structure, and skyrmion lattice would be interesting topics. The search of the hybridized mode in other systems including charge density wave, spin density wave, and ultracold atoms would be important. Last, the effect of hybridization to the lifetime of the magnon and other elementary excitations would be also interesting.

MATERIALS AND METHODS

A single crystal sample was grown by the vertical Bridgman method (*20*). The sample was mounted in a Teflon cell with a deuterated glycerin as a pressure medium so that the horizontal plane is the *ab* plane. The Teflon cell was installed in a piston-cylinder clamped cell made of CuBe alloy. We performed the INS study under pressure using a high-resolution chopper (HRC) spectrometer at J-PARC/MLF in (Japan) (*27*–*29*) and a cold neutron triple-axis spectrometer CTAX at Oak Ridge National Laboratory (ORNL) in USA. The details of the experimental setups including the name of the spectrometer, sample mass, applied pressure, the energy of the neutron, and the temperature are summarized in table S1.

In the HRC experiment, the pressure cell was installed into the closed-cycle ^{4}He cryostat for 0.0 and 0.3 GPa and the ^{3}He cryostat for 1.4 GPa. The energies of the incident neutron were E_i = 8.11 meV for 0.0 GPa, E_i = 5.08 meV for 0.3, and E_i = 3.05 meV for 1.4 GPa. Figure S1 (A and B) shows the INS spectra at 2.7 and 100 K under 0.3 GPa measured at HRC. At 2.7 K, flat excitations are observed at 0.9 and 1.5 meV in addition to the dispersive excitation below 1.0 meV. These flat excitations remain at 100 K, although the dispersive one disappears. The INS spectra at 0.9 and 100 K under 1.4 GPa are shown in fig. S1 (D and E). At 0.9 K, strong intensity is observed around $\boldsymbol{q}$ = 0 in addition to the dispersive excitation, and it remains at 100 K. We thus presume that the data measured at 100 K was the background from the pressure cell and cryostat. Then, the background was subtracted from the data at base temperatures for 0.3 and 1.4 GPa, as shown in fig. S1 (C and F).

In the CTAX experiment, the cell was installed into the ^{4}He cryostat for 0.0, 0.3, 0.6, and 1.4 GPa and ^{3}He cryostat for 0.8, 0.9, and 1.1 GPa. The energy of the final neutron was fixed to be E_f = 3.5 meV. A Hotizontal-focusing analyzer was used to gain high intensity.

SUPPLEMENTARY MATERIALS

Supplementary material for this article is available at http://advances.sciencemag.org/cgi/content/full/5/10/eaaw5639/DC1

Section S1. Supplementary information on experimental methods
Section S2. Energy scheme of Fe^{2+} ion in $CsFeCl_3$
Section S3. ESW theory for triangular antiferromagnet
Section S4. Detailed data analysis for triple-axis spectrometer
Fig. S1. Method of background subtraction for INS spectra.
Fig. S2. Energy scheme of Fe^{2+} ion in $CsFeCl_3$.
Fig. S3. Schematic of hopping and pair creation processes.
Fig. S4. Calculated INS spectra at various pressures.
Fig. S5. Data analysis for triple-axis spectrometer.
Table S1. Summary of experimental setups used for INS measurements under pressures.

Table S2. Summary of parameters obtained from the refinement on the constant q scans [$\boldsymbol{q}$ = (**–k, 2k, 0**)] at 1.4 GPa by Lorentzians convoluted by the experimental resolution functions. References (*31*–*37*)

REFERENCES AND NOTES

1. O. Delaire, J. Ma, K. Marty, A. F. May, M. A. McGuire, M.-H. Du, D. J. Singh, A. Podlesnyak, G. Ehlers, M. D. Lumsden, B. C. Sales, Giant anharmonic phonon scattering in PbTe. *Nat. Mater.* **10**, 614–619 (2011).
2. R. Matsunaga, N. Tsuji, H. Fujita, A. Sugioka, K. Makise, Y. Uzawa, H. Terai, Z. Wang, H. Aoki, R. Shimano, Light-induced collective pseudospin precession resonating with Higgs mode in a superconductor. *Science* **345**, 1145–1149 (2014).
3. J. P. Pouget, B. Hennion, C. Escribefilippini, M. Sato, Neutron-scattering investigations of the Kohn anomaly and of the phase and amplitude charge-density-wave excitations of the blue bronze $K_{0.3}MoO_3$. *Phys. Rev. B* **43**, 8421–8430 (1991).
4. M. Endres, T. Fukuhara, D. Pekker, M. Cheneau, P. Schauβ, C. Gross, E. Demler, S. Kuhr, I. Bloch, The "Higgs" amplitude mode at the two-dimensional superfluid/Mott insulator transition. *Nature* **487**, 454–458 (2012).
5. B. Lake, D. A. Tennant, S. E. Nagler, Novel longitudinal mode in the coupled quantum chain compound $KCuF_3$. *Phys. Rev. Lett.* **85**, 832–835 (2000).
6. A. Zheludev, K. Kakurai, T. Masuda, K. Uchinokura, K. Nakajima, Dominance of the excitation continuum in the longitudinal spectrum of weakly coupled heisenberg S = 1/2 chains. *Phys. Rev. Lett.* **89**, 197205 (2002).
7. C. Rüegg, A. Furrer, D. Sheptyakov, T. Strässle, K. W. Krämer, H.-U. Güdel, L. Mélési, Pressure-induced quantum phase transition in the spin-liquid TlCuCl-3. *Phys. Rev. Lett.* **93**, 257201 (2004).
8. C. Rüegg, B. Normand, M. Matsumoto, A. Furrer, D. F. McMorrow, K. W. Krämer, H.-U. Güdel, S. Gvasaliya, H. Mutka, B. Boehm, Quantum magnets under pressure: Controlling elementary excitations in tlcucl-3. *Phys. Rev. Lett.* **100**, 205701 (2008).
9. P. Merchant, B. Normand, K. Krämer, M. Boehm, D. McMorrow, C. Rüegg, Quantum and classical criticality in a dimerized quantum antiferromagnet. *Nat. Phys.* **10**, 373–379 (2014).
10. A. Jain, M. Krautloher, J. Porras, G. H. Ryu, D. P. Chen, D. L. Abernathy, J. T. Park, A. Ivanov, J. Chaloupka, G. Khaliullin, B. Keimer, B. J. Kim, Higgs mode and its decay in a two-dimensional antiferromagnet. *Nat. Phys.* **13**, 633–637 (2017).
11. T. Hong, M. Matsumoto, Y. Qiu, W. Chen, T. R. Gentile, S. Watson, F. F. Awwadi, M. M. Turnbull, S. E. Dissanayake, H. Agrawal, R. Toft-Petersen, B. Klemke, K. Coester, K. P. Schmidt, D. A. Tennant, Higgs amplitude mode in a two-dimensional quantum antiferromagnet near the quantum critical point. *Nat. Phys.* **13**, 638–642 (2017).
12. S. Ito, N. Kurita, H. Tanaka, S. Ohira-Kawamura, K. Nakajima, S. Itoh, K. Kuwahara, K. Kakurai, Structure of the magnetic excitations in the spin-1/2 triangular-lattice Heisenberg antiferromagnet $Ba_3CoSb_2O_9$. *Nat. Commun.* **8**, 235 (2017).
13. T.-H. Han, J. S. Helton, S. Chu, D. G. Nocera, J. A. Rodriguez-Rivera, C. Broholm, Y. S. Lee, Fractionalized excitations in the spin-liquid state of a kagome-lattice antiferromagnet. *Nature* **492**, 406–410 (2012).
14. B. Fåk, E. Kermarrec, L. Messio, B. Bernu, C. Lhuillier, F. Bert, P. Mendels, B. Koteswararao, F. Bouquet, J. Ollivier, A. D. Hillier, A. Amato, R. H. Colman, A. S. Wills, Kapellasite: A kagome quantum spin liquid with competing interactions. *Phys. Rev. Lett.* **109**, 037208 (2012).
15. J. A. M. Paddison, M. Daum, Z. Dun, G. Ehlers, Y. Liu, M. B. Stone, H. Zhou, M. Mourigal, Continuous excitations of the triangular-lattice quantum spin liquid $YbMgGaO_4$. *Nat. Phys.* **13**, 117–122 (2017).
16. M. Matsumoto, M. Koga, Longitudinal spin-wave mode near quantum critical point due to uniaxial anisotropy. *J. Phys. Soc. Jpn.* **76**, 073709 (2007).
17. M. Matsumoto, Electromagnon as a probe of Higgs (longitudinal) mode in collinear and noncollinear magnetically ordered states. *J. Phys. Soc. Jpn.* **83**, 084704 (2014).
18. M. Mourigal, W. T. Fuhrman, A. L. Chernyshev, M. E. Zhitomirsky, Dynamical structure factor of the triangular-lattice antiferromagnet. *Phys. Rev. B* **88**, 094407 (2013).
19. H. Yoshizawa, W. Kozukue, K. Hirakawa, Neutron scattering study of magnetic excitations in pseudo-one-dimensional singlet ground state ferromagnets $CsFeCl_3$ and $RbFeCl_3$. *J. Phys. Soc. Jpn.* **49**, 144–153 (1980).
20. N. Kurita, H. Tanaka, Magnetic-field– and pressure-induced quantum phase transition in $CsFeCl_3$ proved via magnetization measurements. *Phys. Rev. B* **94**, 104409 (2016).
21. S. Hayashida, O. Zaharko, N. Kurita, H. Tanaka, M. Hagihala, M. Soda, S. Itoh, Y. Uwatoko, T. Masuda, Pressure-induced quantum phase transition in the quantum antiferromagnet $CsFeCl_3$. *Phys. Rev. B* **97**, 140405 (2018).
22. R. Shiina, H. Shiba, P. Thalmeier, A. Takahashi, O. Sakai, Dynamics of multipoles and neutron scattering spectra in quadrupolar ordering phase of CeB_6. *J. Phys. Soc. Jpn.* **72**, 1216–1225 (2003).
23. S. Sachdev, R. N. Bhatt, Bond-operator representation of quantum spins: Mean-field theory of frustrated quantum Heisenberg antiferromagnets. *Phys. Rev. B* **41**, 9323–9329 (1990).
24. T. Sommer, M. Vojta, K. W. Becker, Magnetic properties and spin waves of bilayer magnets in a uniform field. *Eur. Phys. J. B* **23**, 329–339 (2001).
25. M. Matsumoto, B. Normand, T. M. Rice, M. Sigrist, Magnon dispersion in the field-induced magnetically ordered phase of $TlCuCl_3$. *Phys. Rev. Lett.* **89**, 077203 (2002).
26. M. Matsumoto, B. Normand, T. M. Rice, M. Sigrist, Field- and pressure-induced magnetic quantum phase transitions in $TlCuCl_3$. *Phys. Rev. B* **69**, 054423 (2004).
27. S. Itoh, T. Yokoo, S. Satoh, S.-i. Yano, D. Kawana, J. Suzuki, T. J. Sato, High resolution chopper spectrometer (HRC) at J-PARC. *Nucl. Instrum. Methods Phys. Res. Sect. A* **631**, 90–97 (2011).
28. S.-i. Yano, S. Itoh, S. Satoh, T. Yokoo, D. Kawana, T. J. Sato, Data acquisition system for high resolution chopper spectrometer (HRC) at J-PARC. *Nucl. Instrum. Methods Phys. Res. Sect. A* **654**, 421–426 (2011).
29. S. Itoh, T. Yokoo, D. Kawana, H. Yoshizawa, T. Masuda, M. Soda, T. J. Sato, S. Satoh, M. Sakaguchi, S. Muto, Progress in high resolution chopper spectrometer, HRC. *J. Phys. Soc. Jpn.* **82**, SA033 (2013).
30. A. Kohne, E. Kemnitz, H. J. Mattausch, A. Simon, Crystal structure of caesium trichloroferrate(II). $CsFeCl_3$. *Z. Kristallogr.* **203**, 316–317 (1993).
31. K. Inomata, T. Oguchi, Theory of Magnetism in $FeCl_2$ $2H_2O$. *J. Phys. Soc. Jpn.* **23**, 765–770 (1967).
32. M. Eibschütz, M. E. Lines, R. C. Sherwood, Magnetism in orbitally unquenched chainar compounds. II. The ferromagnetic case: $RbFeCl_3$. *Phys. Rev. B* **11**, 4595–4605 (1975).
33. T. Nikuni, H. Shiba, Quantum fluctuations and magnetic structures of $CsCuCl_3$ in high magnetic field. *J. Phys. Soc. Jpn.* **62**, 3268–3276 (1993).
34. A. L. Chernyshev, M. E. Zhitomirsky, Spin waves in a triangular lattice antiferromagnet: Decays, spectrum renormalization, and singularities. *Phys. Rev. B* **79**, 144416 (2009).
35. R. Shiina, M. Matsumoto, M. Koga, Crystal-field excitations, magnetic-field-induced phase transition and neutron-scattering spectra in $PrOs_4SB_{12}$. *J. Phys. Soc. Jpn.* **73**, 3453–3461 (2004).
36. M. Matsumoto, T. Shoji, M. Koga, Theory of magnetic excitations and electron spin resonance for anisotropic spin dimer systems. *J. Phys. Soc. Jpn.* **77**, 074712 (2008).
37. H. Kuroe, N. Takami, N. Niwa, T. Sekine, M. Matsumoto, F. Yamada, H. Tanaka, K. Takemura, Longitudinal magnetic excitation in $KCuCl_3$ studied by Raman scattering under hydrostatic pressures. *J. Phys. Conf. Ser.* **400**, 032042 (2012).

Acknowledgments: We are grateful to D. Kawana, T. Asami, R. Sugiura, A. A. Aczel, S. Asai, and S. Hasegawa for supporting us in the neutron scattering experiments. We greatly appreciate M. Takigawa for fruitful discussions. The neutron scattering experiment at the HRC was approved by the Neutron Scattering Program Advisory Committee of IMSS, KEK (proposals nos. 2015S01, 2016S01, and 2017S01), and ISSP. A portion of this research used resources at the High Flux Isotope Reactor, a DOE Office of Science User Facility operated by the Oak Ridge National Laboratory. **Funding:** Travel expenses for the neutron scattering experiments performed using CTAX at ORNL, USA was supported by the U.S.–Japan Cooperative Research Program on Neutron Scattering (proposal no. 2017-21). S.H. was supported by the Japan Society for the Promotion of Science through the Leading Graduate Schools (MERIT). M.M. was supported by JSPS KAKENHI grant number 17K05516, and N.K. and H.T. were supported by JSPS KAKENHI grant number 16K05414. **Author contributions:** T.M. conceived the project; N.K. and H.T. prepared the samples; S.H. and T.M. performed neutron experiments under pressure with the help of M.H., S.I., T.H., M.S., and Y.U.; M.M. performed theoretical calculations; and S.H. analyzed the data. All authors contributed to writing of the manuscript. **Competing interests:** The authors declare that they have no competing interests. **Data and materials availability:** All data needed to evaluate the conclusions in the paper are present in the paper and/or the Supplementary Materials. Additional data related to this paper may be requested from the authors.

Submitted 6 January 2019
Accepted 25 September 2019
Published 18 October 2019
10.1126/sciadv.aaw5639

Citation: S. Hayashida, M. Matsumoto, M. Hagihala, N. Kurita, H. Tanaka, S. Itoh, T. Hong, M. Soda, Y. Uwatoko, T. Masuda, Novel excitations near quantum criticality in geometrically frustrated antiferromagnet $CsFeCl_3$. *Sci. Adv.* **5**, eaaw5639 (2019).